

GDAnet enables cross-scale prediction of granular flow from static snapshots to dynamic space–time

Xin Zhang(张馨), Xinyao Wang(王新尧), Yanjun Liu(刘彦君), Wen Zheng(郑文)
Citation: Chin. Phys. B. 35, 094501 (2026). DOI: 10.1088/1674-1056/ae1de8 |
CSTR: 32038.14.CPB.ae1de8
http://cpb.iphy.ac.cn; http://iopscience.iop.org/cpb

What follows is a list of articles you may be interested in

Exploring protein conformations by cluster-guided iterative multiple independent molecular dynamics simulations

Chengtao Ding(丁成涛), Guanglin Chen(陈光临), Qingguo Gong(龚庆国), Zhiyong Zhang(张志勇)
Chin. Phys. B. 35, 058702 (2026). DOI: 10.1088/1674-1056/ae0898 | CSTR: 32038.14.CPB.ae0898

Accurate prediction of essential proteins using ensemble machine learning

Dezhi Lu(鲁德志), Hao Wu(吴浩), Yutong Hou(侯俞彤), Yuncheng Wu(吴云成), Yuanyuan Liu(刘媛媛), Jinwu Wang(王金武)
Chin. Phys. B. 34, 018901 (2025). DOI: 10.1088/1674-1056/ad8db2 | CSTR: 32038.14.CPB.ad886a

Learning physical states of bulk crystalline materials from atomic trajectories in molecular dynamics simulation

Tian-Shou Liang(梁添寿), Peng-Peng Shi(时朋朋), San-Qing Su(苏三庆), Zhi Zeng(曾志)
Chin. Phys. B. 31, 126402 (2022). DOI: 10.1088/1674-1056/ac98a4

Development of an electronic stopping power model based on deep learning and its application in ion range prediction

Xun Guo(郭寻), Hao Wang(王浩), Changkai Li(李长楷), Shijun Zhao(赵仕俊), Ke Jin(靳柯), Jianming Xue(薛建明)
Chin. Phys. B. 31, 073402 (2022). DOI: 10.1088/1674-1056/ac4e0c

---

GDAnet enables cross-scale prediction of granular flow from static snapshots to dynamic space–time

Xin Zhang(张馨)[1], Xinyao Wang(王新尧)[2,†], Yanjun Liu(刘彦君)[1], and Wen Zheng(郑文)[1,2]

[1] *Institute of Public-Safety and Big Data, College of Computer Science and Technology (College of Data Science), Taiyuan University of Technology, Jinzhong* 030600, *China*

[2] *Key Laboratory for Satellite Digitalization Technology, Institute of Microsatellite Innovation, Chinese Academy of Sciences, Shanghai* 201304, *China*

(Received 29 July 2025; revised manuscript received 8 October 2025; accepted manuscript online 11 November 2025)

Accurate prediction of granular flow in funnels remains a central challenge in granular mechanics and materials engineering. Conventional methods depend heavily on high-dimensional particle coordinate–velocity fields, which are costly to acquire, making it difficult to balance predictive accuracy and timeliness. This study constructs GDAnet, a deep learning framework that uses images as its input to extract key features of granular distributions from static snapshots and predict flow patterns across temporal intervals. Experimental results demonstrate that GDAnet achieves a coefficient of determination (R^2) of 0.992 in single-frame prediction tasks, substantially outperforming existing baseline models. In modeling temporal evolution, the framework achieves more than 90% precision in classifying various flow stages (*e.g.* falling, flowing, and blocking) and accurately predicts flow rate variations across different friction coefficients, both with and without clogging conditions. GDAnet overcomes the limitations of traditional numerical methods in computational efficiency and scalability through its image-to-motion learning paradigm, offering a novel technical pathway for granular flow research.

Keywords: funnel granular flow, molecular dynamics simulation, deep learning, image prediction

PACS: 45.70.–n, 45.70.Vn, 47.57.Gc, 47.80.Jk

DOI: 10.1088/1674-1056/ae1de8 **CSTR:** 32038.14.CPB.ae1de8

1. Introduction

In the realm of contemporary industrial production, the study of granular flow dynamics has ascended to the forefront as an interdisciplinary focal point with the continuous improvement of technological innovation and production efficiency. This field has shown its far-reaching application potential and scientific value in many key industries, such as chemical engineering, pharmaceutical industry, food processing, *etc*.[1,2] The precise control and optimization of granular flow are essential for enhancing product quality, reducing production expenses, and ensuring the safety and sustainability of manufacturing processes. Among various devices for granular flow control, the conical funnel is an essential component due to its distinctive geometry and operational simplicity. The characteristics of granular flow within the conical funnel, encompassing flow patterns, velocity profiles, and granular interactions, critically influence the production process's efficiency and effectiveness.[3] A comprehensive investigation into the dynamics of granular flow within the conical funnel not only elucidates the foundational principles governing granular flow but also offers significant theoretical insights and practical implications, guiding engineering design and enhancing production methodologies. The conventional research approach predominantly employs the development of physical models and experimental methodologies.[4,5] Since 1957, Adler and his colleagues have been pioneering the construction of molecular dynamics models, enabling precise tracking of granule trajectories.[6] The advent of the large-scale atomic/molecular massively parallel simulator (LAMMPS), developed by Sandia National Laboratories in the USA, has emerged as a preeminent and efficient tool for large-scale molecular dynamics (MD) simulations, offering unparalleled comprehensiveness and efficacy.[7]

With the development of MD simulations, we have access to a vast array of experimental data concerning funnel granular flow. This wealth of information offers fresh perspectives and insights. However, the efficient processing and analysis of this data pose a formidable challenge, as the precision and reliability of MD simulations are inevitably circumscribed by the intricacies of the model and the experimental conditions. The extensive computational volume results in sluggish simulation speeds and limits the scope of simulations.[8] Consequently, the pursuit of more efficient and precise methods for studying conical funnel granular flow has emerged as a prominent research focus.[9] Real-time, non-intrusive observations (high-speed videography) are the primary means of obtaining granular flow states in industrial sites, but they provide image sequences rather than direct particle coordinate/velocity data. Therefore, the development of methods that can learn and predict the dynamic behavior of granular flow directly

[†]Corresponding author. E-mail: wangxinyao@microsate.ac.cn

© 2026 Chinese Physical Society and IOP Publishing Ltd. All rights, including for text and data mining, AI training, and similar technologies, are reserved.

from visual image features not only circumvents the computational bottleneck of MD simulation, but also directly interfaces with the observation method of actual industrial scenes, which has significant advantages for practical applications. In recent years, the incorporation of machine learning techniques has been aimed at enhancing the computational efficiency of MD simulations.[10] Initially, Mujumdar *et al*. forecasted the mixing and separation dynamics of granular flow within a system equipped with an oscillating fan vessel, employing an artificial neural network (ANN) in conjunction with numerical data from the discrete element method (DEM).[11] Cui *et al*. introduced a novel framework that integrates DEM data with a deep neural network (DNN), facilitating the design of a double-barrier system.[12] Deep learning, an influential data analytics tool, is capable of discerning valuable feature representations and patterns from extensive datasets, offering innovative approaches and methodologies for the study of funnel granular flow.[13–15] Furthermore, it serves as a bridge between disparate simulation scales, significantly alleviating the computational load while preserving predictive accuracy.[16,17]

Despite extensive research integrating MD simulations with deep learning methods, the majority of granular behavior predictions continue to depend predominantly on simulated data over actual images.[18] Nonetheless, in contrast to processed data, continuous real-time imagery offers a more direct and immediate representation of outcomes, eliminating the need for additional data extraction procedures.[19–21] Concurrently, deep learning algorithms have shown remarkable proficiency in the domain of image recognition. Consequently, it is a plausible hypothesis that convolutional neural networks (CNNs) could serve as a viable alternative for precisely modeling and forecasting the dynamics of particulate motion, potentially replacing certain facets of existing physical simulation techniques.[22,23]

The aim of this paper is to develop a deep learning-based image-driven method, capable of extracting key spatio-temporal information directly from static snapshots of granular flow, to enable cross-scale prediction of funnel granular flow from transient states (outflow time points) to fully dynamic evolutionary processes (flow phases, clogging states). In this process, we rely on LAMMPS, a powerful simulation tool, to simulate images of transient granular flows.[7] With the image data generated from these simulations, we were able to gain insight into the dynamics of the granular flow, providing a solid foundation for subsequent analysis and prediction. In order to achieve accurate prediction of particle flow behaviour, we construct an improved model based on the AlexNet model in CNN, in which a depth expectation (DEX) module is added. The improvement fully considers the importance of the time factor in granular flow analysis. We consider time points as key variables in segmented regression, which enables us to capture time-dependent features. In this way, the model can make accurate point-to-point predictions of the outflow time of granular flows using only image data. In addition to point-in-time prediction, we also utilise the model to further extend the scope of prediction. The model is known for its excellent feature extraction and classification capabilities, which we have optimised and adapted to make it better suited to the task of predicting the extent of granular flow. With this model, we can make predictions about the overall flow extent of the granular flow, providing a more comprehensive view to understand the dynamic behaviour of the particulate flow. In this study, we have successfully achieved accurate prediction of granular flow behaviour by combining a new approach of deep learning with classical physical simulation tools. This not only expands the application scope of deep learning in physics, but also provides new ideas and methods for solving other similar complex physics problems.

2. Method

2.1. GDAnet model construction

2.1.1. AlexNet

AlexNet, a pioneering deep convolutional neural network, is extensively utilized for image classification within the realm of computer vision, and it secured its place as the inaugural deep learning model to attain significant acclaim in the ImageNet Large Scale Visual Recognition Challenge.[24,25]

The network architecture presented in this paper adopts the AlexNet framework, employing a nonlinear and unsaturated rectified linear unit (ReLU) as the activation function, which exhibits a significantly reduced rate of gradient decay compared to the saturated nonlinear functions, such as the sigmoid and hyperbolic tangent (tanh) functions, prevalent in conventional neural networks.[26] AlexNet operates across two graphics processing units (GPUs), with each GPU handling half of the network's computational tasks, while employing local response normalization (LRN), a technique that obviates the need for input normalization. Each GPU is tasked with processing half of the network's operations, utilizing LRN, which facilitates the ReLU function without necessitating prior input normalization. However, Krizhevskii *et al*. discovered that integrating LRN with the ReLU layer introduces a form of lateral inhibition, thus enhancing the network's generalization capabilities.[27] The pooling strategy employs an overlapping pooling technique, where the pooling window exceeds the stride size, resulting in overlapping pooling regions. This method of overlapping pooling yields superior outcomes compared to traditional nonoverlapping pooling and mitigates the overfitting phenomenon. A dropout technique, which randomly deactivates neurons, is implemented in the fully connected initial layers to reduce overfitting.[28]

2.1.2. DEX

Predicting the exact time point of a granular flow is a continuous regression problem. Direct regression may have difficulty in capturing complex temporal dependencies. The DEX module transforms continuous time prediction into a multi-classification problem with ordered attributes. This utilizes the powerful feature extraction capabilities of classification networks, while effectively reducing regression errors by calculating the expected value of the probability of each time point and fusing the discrete classification results into continuous, physically interpretable point-in-time predictions. The approach introduced in this paper adheres to the schematic flow depicted in Fig. 1. During regression training, the output layer is configured to consist of distinct neurons, each associated with specific regression time points. For classification training, the output layer comprises 160 neurons, mapped to natural numbers ranging from 0 to 159, facilitating the discretization of temporal category labels.[29] The quantity strikes a good balance between computational efficiency and prediction accuracy.

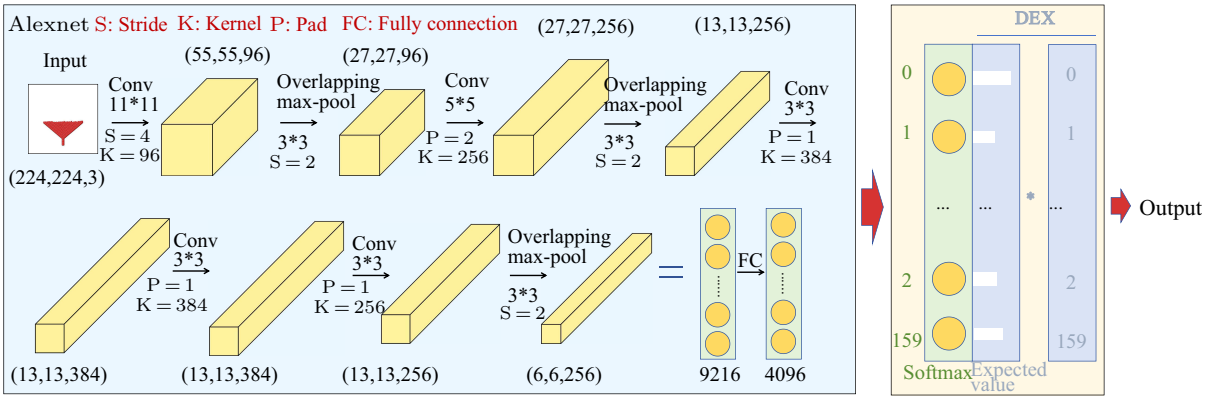


Fig. 1. Diagram of the structure of the GDAnet model.

Temporal estimation is conceptualized as a form of segmented regression, characterized by discrete categorization with multiple distinct value labels. An increased number of classes results in a reduced discretization error for the regression signal. In this study's example, a one-dimensional regression problem, time is sampled from a continuous signal ranging from 0 to 159. Enhancement of the regression time classification formula can be achieved by substantially increasing the class count, thereby improving signal approximation and facilitating recovery through the aggregation of neuron outputs. Expanding the class count necessitates an adequate number of training samples per class and elevates the risk of overfitting to the training time distribution, as well as the potential for improper training of samples attributable to sample scarcity or imbalance. Following several preliminary experiments, the decision was made to utilize 160 time periods. To enhance the precision of predictions, the Softmax expectation was ultimately computed.[30] Specifically, once a prediction is obtained using the AlexNet network and the probabilities for each category are determined via Softmax computation, each category's probability is multiplied by its corresponding value. This process yields the final time-accurate outcome, transcending a mere probability-maximum result.

2.1.3. GDAnet

The aforementioned AlexNet model is integrated with a fully connected network to construct the foundational AlexNet architecture, the architecture of which is illustrated in Fig. 1. In summary, the left component employs the AlexNet model to extract features from the input image; concurrently, the lower segment of the right component leverages the fully connected layer to analyze these extracted features.

The GDAnet model is an extension of the AlexNet model and retains its classification architecture with the incorporation of the calculation of the maximum expected value (E) of Softmax at its culmination, as shown in Eq. (1). Utilizing 160 time points in this research, the output layer in Eq. (1), denoted as $p = 0, 1, 2, \ldots, 159$, constitutes a 160-dimensional array representing the Softmax output probabilities $p_i \in P$, where y_i corresponds to the probability associated with each time point for category i.

$$E(P) = \sum_{i=0}^{159} y_i p_i. \tag{1}$$

Subsequently, by employing backpropagation of the discrepancy between the expected values and the actual labels, the estimates of maximum expected values can be optimized, thereby enhancing network performance. The estimation of temporal points is treated as a form of discrete classification, characterized by a multitude of discrete value labels, and an increased number of classes leads to a reduction in the discretization error of the regression signal. Consequently, this refined model is suitable for predicting time points by processing arbitrary granular flow images through the model.

The core innovation of GDAnet lies in its spatio-temporal feature decoupling architecture, where the AlexNet backbone network focuses on extracting key spatial structural features (particle distribution density, stacking morphology near the funnel opening) from a single-frame image, while the DEX module is responsible for learning the complex mapping relationship between these spatial features and dynamic evolutionary time. This decoupled design enables it to perform both static time-point prediction (outputting a time value) and dynamic stage classification (outputting a stage label) tasks based on single-frame images, realizing cross-scale prediction from static snapshots to dynamic spatio-temporal. Consequently, the granular outflow time within the conical funnel can be prognosticated by submitting any arbitrary granular flow image to the proposed model. In addition, the temporal stage range of the depicted flow can be predicted.

2.2. Granular flow image construction

The LAMMPS simulation operates on the principle of molecular dynamics, wherein the trajectory of each particle is determined by integrating Newton's equations of motion, and the forces exerted on each atom are computed based on their instantaneous positions and velocities, thereby yielding the subsequent acceleration and updated positions of each atom. This iterative process generates a time-evolving sequence, encapsulating the dynamic behavior of the system as a whole. The specific formulas are

$$m_i \frac{\mathrm{d}V_i}{\mathrm{d}t} = \sum_{j=1}^{n} \boldsymbol{F}_{ji}^{C} + m_i g, \tag{2}$$

$$I_i \frac{\mathrm{d}\omega_i}{\mathrm{d}t} = \sum_{j=1}^{n} \boldsymbol{r}_{ij} \times \boldsymbol{F}_{ji}^{C}, \tag{3}$$

where m_i, I_i, V_i, ω_i are the mass, inertial distance, translational velocity, and rotational velocity of the granular, respectively. $\boldsymbol{r}_{ij}$ is the vector of particle 'i' pointing towards 'j'. The forces involved include the gravitational force mi,g, and the contact force between the particle and or between the particle and the container wall. By solving Eqs. (2) and (3), the trajectory, velocity, and force of each particle in the system can be tracked with certainty.

For the modelling of contact friction we used the Hertzian style (4)

$$\begin{aligned} F_{hz} &= \sqrt{\delta}\sqrt{\frac{R_i R_j}{R_i + R_j}} F_{hk} \\ &= \sqrt{\delta}\sqrt{\frac{R_i R_j}{R_i + R_j}} [(k_n \delta \boldsymbol{n}_{ij} - m_{\mathrm{eff}} \gamma_n \boldsymbol{v}_n) \\ &\quad - (k_t \Delta \boldsymbol{s}_t + m_{\mathrm{eff}} \gamma_t \boldsymbol{v}_t)], \end{aligned} \tag{4}$$

$\delta = d - r$, meaning the overlap distance of the 2 particles. k_n is the elastic constant for normal contact, kt is the elastic constant for tangential contact, γ_n is the viscoelastic damping constant for normal contact, γ_t is the viscoelastic damping constant for tangential contact, m_{eff} is the effective mass of the 2 particles of mass m_i and m_j, $\Delta \boldsymbol{s}_t$ is the vector of tangential displacements between the 2 particles, which is truncated to satisfy the frictional yield criterion, $\boldsymbol{n}_{ij}$ is the unit vector along the line joining the centres of the 2 particles, $\boldsymbol{v}_n$ is the normal component of the relative velocity of the 2 particles, and $\boldsymbol{v}_t$ is the tangential component of the relative velocity of the 2 particles.

This process is repeated to form a sequence that evolves over time, thus simulating the dynamic behavior of the whole system. Because there are many factors affecting the granular flow in the funnel, the physical properties of the particles, the geometry and size of the funnel, and the external addition conditions will have a critical impact on the velocity, distribution, and flow mode of the granular flow. In order to verify the generalization ability of the model, we debugged the inter-particle friction coefficients (μ) during the granular flow, and took the μ of 0.0001, 0.1, 0.2, 0.3, 0.4 for the simulation, respectively. The simulation parameters in this paper are shown in Table 1.

The simulation process is structured into four distinct phases: initial filling, stable relaxation, fast flow, and end-of-flow. In the initial filling phase, 1000 particles are introduced into the funnel from the top in a random manner under the influence of gravity. During the stable relaxation phase, the discharge orifices at the funnel's base are sealed, allowing the particles to accumulate and reach a static state over an adequate duration. In the flow phase, the orifices are opened, enabling the particles to exit freely under gravitational influence; however, there exists the potential for blockages during this phase, hindering continuous flow under specific conditions. Consequently, LAMMPS simulations are capable of producing not only instantaneous granular flow images for predictive analysis, but also images that capture granular flow throughout various stages of the process.

Table 1. Table of data set parameters.

Parameter	Value
Particle diameter d	0.5
Number of particles	1000
Young's modulus E	10^5
Friction coefficient μ	0.001, 0.1, 0.2, 0.3, 0.4
Coefficient of recovery	0.2
Funnel diameter D	20d
Funnel opening diameter	2,0.8
Angle of funnel	45
Timestep (s)	10^{-4}

2.3. Experimental environment

The model training and testing for this study are conducted on a server-based platform. The server operates on the CentOS 7.9 operating system, equipped with 8 NVIDIA V100 GPUs, each possessing 16160 MiB of video memory,

CUDA version 10.2, and cuDNN version 8.4.0. Throughout the training process, the input images are uniformly resized to a dimension of $224 \times 224 \times 3$ pixels, utilizing 2 GPUs, with a batch size of 32 and a total of 100 epochs, and an initial learning rate of 0.01 is specified. The learning rate is subject to dynamic adjustment throughout the training process.

3. Experiments and results

3.1. Image data acquisition and pre-processing

Initially, 16200 frontal-view snapshots of granular flow were randomly sampled at varying instantaneous time steps across 100 distinct LAMMPS simulation instances, each initialized with unique random seed numbers. Subsequently, a timestamp was assigned to each snapshot based on the simulation-determined time step required for the complete efflux of granules from the funnel. The timestamp of each snapshot labels the simulation time from that moment until the particles completely flow out of the funnel, a key dynamic process physical quantity. Stage labels are then manually categorized based on the macroscopic physical state of the granular flow (initial filling, stable relaxation, rapid flow, terminal flow, and blockage state).

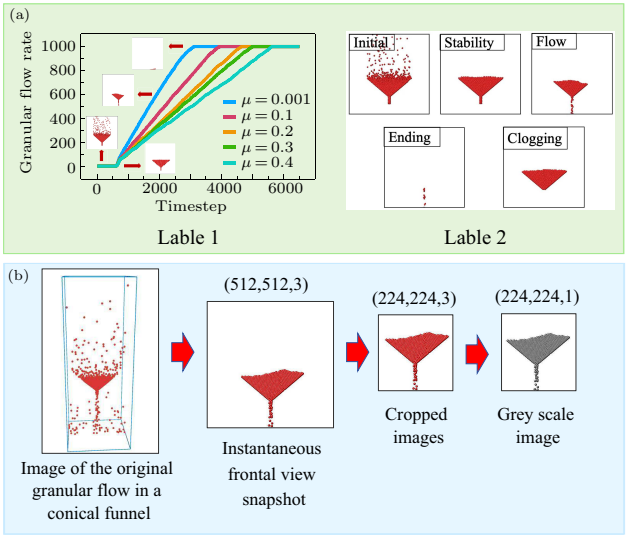


Fig. 2. Panel (a) shows two separate labels given to the dataset. Lable 1 is the first label that represents the timestamps given to the granular flow time pictures for each time step of the flow process with different friction simulation effects. Lable 2 is the second label that categorizes all the pictures appearing throughout the flow process into five different categories of states (initial state, stable state, flow dynamic state, ending state, blocked state). (b) Dataset preprocessing process. Conversion from 3d image to 2d then cropping image and grayscaling.

Subsequently, each snapshot is converted into a three-dimensional (3D) data matrix. Given that the original image dimensions are $512 \times 512 \times 3$, to mitigate overfitting, a data augmentation technique is employed, thereby enhancing the diversity of the training dataset and bolstering the model's generalization capabilities through various image transformations, including rotation, flipping, and cropping. For this research, the peripheral regions of the images are cropped to a size of $224 \times 224 \times 3$, which are subsequently desaturated to grayscale using deep learning algorithms and reshaped into a one-dimensional (1D) matrix for immediate use in the subsequent computational processes. As depicted in Fig. 2.

3.2. Training model selection and evaluation metrics

The preprocessed images are randomly allocated into three distinct groups: a training set (60%), a testing set (20%), and a cross-validation set (20%). Subsequently, four CNN models, AlexNet, VGGNet, ResNet, and GDAnet, are trained on the initial dataset comprising instantaneous granular flow snapshots. These models are then tested and validated, with their predictions quantitatively compared against the cross-validation dataset using metrics such as accuracy (ACC), mean absolute error (MAE), root-mean-square error (RMSE), and coefficient of determination (R^2), as defined by Eqs. (5)–(7). The MAE is calculated as the average of the absolute differences between the estimated and actual times, preventing offsetting errors. The RMSE, normalized by the square root of the sample size, accounts for the magnitude of errors without bias from sample count. For the R^2, when comparing models on datasets of varying scales, a reference model is utilized to facilitate a more accurate comparison; typically, a higher R^2 value suggests a better fit.

$$\mathrm{MAE} = \frac{1}{m}\sum_{i=1}^{m}|y_i - \hat{y}_i|, \tag{5}$$

$$\mathrm{RMSE} = \sqrt{\frac{1}{m}\sum_{i=1}^{m}(y_i - \hat{y}_i)^2}, \tag{6}$$

$$R^2 = 1 - \frac{\sum_{i=1}^{m}(y_i - \hat{y}_i)^2}{\sum_{i=1}^{m}(y_i - \bar{y}_i)^2}, \tag{7}$$

In the given context, m represents the number of predictions, which corresponds to the prediction length or the total number of time steps or samples being predicted. Additionally, y_i denotes the observed value for a given time step or sample i, $\hat{y}_i$ is the predicted value for the same instance, and $\bar{y}$ signifies the average value of the observed values across all predictions.

In the domain of physical image classification, this study employs a multifaceted evaluation approach to ascertain model performance. The primary metric is the probability of accurate classification per image category. Additionally, the receiver operating characteristic (ROC) curve and the area under the ROC curve (AUC) are utilized to gauge classification accuracy across different models. The ROC curve is generated by ranking samples according to prediction scores, sequentially considering them as positive cases, and plotting the true positive rate (TPR) against the false positive rate (FPR). The AUC, scaled from 0 to 1, offers a direct measure of classification quality, with higher values indicating enhanced performance.

In this context, true positives (TP) are correctly identified positive instances, false positives (FP) are incorrectly identified positive instances, true negatives (TN) are correctly identified negative instances, and false negatives (FN) are incorrectly identified negative instances. Consequently, the AUC is derived from these values as follows:

$$\mathrm{AUC} = \frac{\sum_{i\in \text{ positiveClass}} \mathrm{rank}_i - M(1+M)/2}{M \times N}. \tag{8}$$

In the calculation of AUC, M denotes the count of positive samples, N signifies the count of negative samples, and rank_i is the ordinal position assigned to sample i based on the model's predicted probabilities.

3.3. Predicted results

3.3.1. Granular outflow time point prediction effects

As depicted in Fig. 3, we compare the predicted granular outflow time within the funnel to the actual and observed values, and the corresponding decision coefficients are computed and displayed in the inset. These results conclusively show that the proposed GDAnet model typically exhibits superior predictive capability for the outflow time point associated with any instantaneous image of the granular flow in the conical funnel, outperforming other models, and indicate a strong correlation between the predicted and actual values. The primary deviation is observed near the origin, attributed to the limited data available at this stage when the granular material is not fully filled.

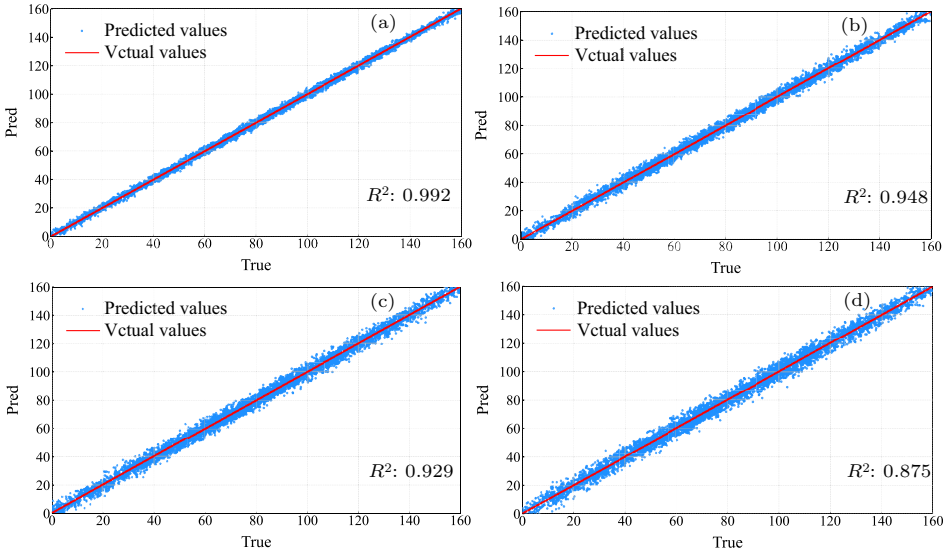


Fig. 3. Results of the comparison between the actual time point of funnel particle outflow and the predicted time point on the test set. Panel (a) shows the GDAnet model results. Panel (b) shows the AlexNet model results. Panel (c) shows the VggNet model results, and panel (d) shows the ResNet results.

Although the scatter plots in Fig. 3 appear visually similar across models, the quantitative metrics in Table 2 reveal that ResNet exhibits significantly larger prediction errors (MAE = 2.790, RMSE = 3.824) compared to GDAnet, AlexNet, and VGGNet. This is attributed to ResNet's deeper architecture, which may overfit on limited training data or fail to capture granular flow features effectively without sufficient regularization or tuning. The similar visual trends in Fig. 3(d) are misleading due to the scale of the y-axis, which compresses the error distribution. Thus, quantitative evaluation is essential for accurate model comparison.

We then test and validate the four rigorously trained models on this dataset, comparing their predictions to the actual values, with further quantitative comparisons detailed in Table 2. The GDAnet hybrid model, in contrast, excels in this dataset's task by amalgamating the strengths of both models, exhibiting the smallest mean absolute error (MAE), root mean square error (RMSE), and the highest coefficient of determination (R^2), and is deemed optimal for predicting granular flow within conical funnels. The very high coefficient of determination achieved by GDAnet ($R^2 = 0.992$) shows that the model can predict the subsequent granular flow time extremely accurately from a single still image. This means that in industrial processes, a simple snapshot can be used to assess in real time the expected discharge efficiency in the current material state, providing critical information for process control.

Table 2. Quantitative comparison of predictive performance of four CNN models.

	MAE	MSE	RMSE	R^2
GDAnet	0.311	0.146	0.382	0.992
AlexNet	0.643	0.480	0.693	0.929
ResNet	2.790	14.622	3.824	0.875
VggNet	0.358	0.247	0.497	0.948

3.3.2. Effectiveness of granular flow stage prediction

The granular flow within a conical funnel is categorized into five predictive stages: initial influx stage, steady relaxation stage, continuous flow stage, end-of-flow stage, and clogged state.

In the initial influx stage, grains start to cascade into the funnel, maintaining a relatively smooth flow due to the slow flow rate and minor interactions among grains. As the quantity of granules increases, the flow rate gradually accelerates, yet it settles into a stable phase as the granular material accumulates. In the stable relaxation stage, the particle count continues to escalate, and the flow rate sustains its stability; during which the interaction among the granules starts to display a discernible pattern, enhancing the flow's regularity. This phase is typically enduring. The concentration of granules and the flow velocity peak in the sustained flow stage, with the flow dynamics becoming increasingly intricate due to intense interactions among granular constituents. The internal pressure and friction within the funnel are elevated, potentially resulting in funnel wear and blockage. Commencing at the end of the flow phase, the granular flow begins to decelerate and ultimately ceases, with the residual granular matter commencing gradual deposition, forming a relatively stable sedimentation layer. In the granular blockage state, once the granular flow within the funnel ceases completely, the funnel becomes obstructed. The funnel, under this condition, is incapable of accepting further granular inflow.

Table 3 presents the confusion matrix of the GDAnet model for the five-stage classification task. Each row represents the true class, and each column represents the predicted class. The diagonal elements indicate the classification accuracy for each stage, while off-diagonal elements represent misclassification rates. It is observed that the likelihood of precise categorization exceeds 0.75. This shows superior capability in forecasting the range of granular flow within the funnel. There is a small amount of confusion in the model in distinguishing between approaching phases (0.97% misclassification of the 'stabilization' phase as 'blockage'), reflecting the possible physical ambiguity or transitory nature of these phase transition boundaries.

Table 3. Prediction probability of GDAnet five-stage classification.

	True-initial	True-stability	True-flow	True-ending	True-clogging
Pred-initial	0.997	0.00157	0.00148	0.000122	1.17×10^{-7}
Pred-stability	0.00434	0.981	0.0097	3.27×10^{-5}	0.00541
Pred-flow	5.59×10^{-8}	9.77×10^{-6}	0.998	0.00205	5.14×10^{-8}
Pred-ending	0.0024	0.00092	0.226	0.771	2.72×10^{-5}
Pred-clogging	1.18×10^{-5}	0.00137	0.000284	2.07×10^{-6}	0.998

As shown in Fig. 4, the ROC curve is primarily utilized to assess the classification model's performance. The horizontal axis represents the FPR, and the vertical axis denotes the TPR. Distinct colors differentiate the data points for each category, facilitating the observation of individual category performance. According to the visual data, it is evident that each class is associated with its distinct ROC curve, with the respective area under the curve (AUC value) indicated. Notably, for class 0, the AUC value is 0.99, while classes 1 and 2 each exhibit an AUC value of 0.97, and class 3 possesses an AUC value of 0.96. Class 4, conversely, presents an AUC value of 0.95. An AUC value closer to 1 indicates superior classification performance by the model.

Synthesizing this data, it can be concluded that across all classes, the classification model exhibits exemplary performance, particularly for class 0 with an AUC value of 0.99, demonstrating exceptionally high classification precision. Additionally, the AUC values for all remaining classes surpass 0.95, suggesting robust generalization capabilities and adeptness in managing diverse data categories. Collectively, these findings underscore the GDAnet model's enhanced predictive capacity for granular flow within funnels, signifying its capability to forecast the entire granular flow trajectory rather than being confined to discrete temporal junctures. The model's ability to identify with high accuracy the macroscopic stage in which the granular flow is located provides a direct basis for real-time monitoring of the system's state (whether it is functioning properly or not and whether there is a risk of clogging).

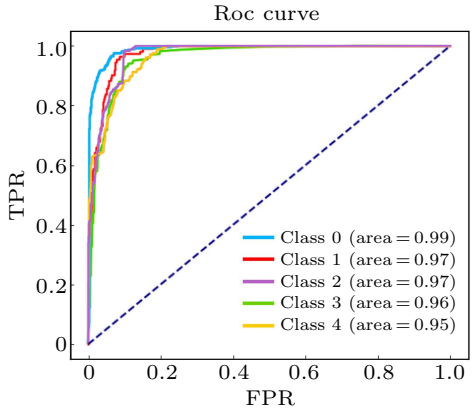


Fig. 4. Comparison of predicted results of ROC curves for five stages of granular flow, where class 0 is the initial filling stage, class 1 is the stabilization stage, class 2 is the flow stage, class 3 is the end of flow stage, and class 4 is the clogging state.

The success of stage prediction, combined with point-in-time prediction, fully validates the ability of the GDAnet model to achieve cross-scale prediction from a single frame of the image: not only can a specific physical quantity (time) be predicted, but also the macroscopic state of the entire dynamic evolution process can be identified and predicted.

3.3.3. Prediction of granular flow with or without clogging effects

Through the prediction analysis of the dynamic process in the previous step, we found that the funnel aperture size of the research setup in the presence of friction occasionally resulted in a situation where particles clogged in the funnel mouth and could not flow out. In order to verify whether the clogging state would have an effect on the prediction effect, we adjusted the funnel aperture size and trained the prediction for the non-clogged system with a radius of 2.0 at the funnel mouth and the system in the presence of clogging with a reduced radius of 0.8, respectively. The left panel of Fig. 5 (without clogging, large aperture) demonstrates the fitted curves where the predicted time points highly coincide with the actual time points. The right figure (with clogging, small aperture), on the other hand, shows that although there is a prediction bias caused by clogging (the actual outflow time is infinitely prolonged, and the prediction value will be saturated or the error will be increased), the overall distribution trend of the model's prediction value (a large number of prediction points are concentrated in the region of high time values) or an abnormal increase in the prediction time point can clearly indicate that the system is in or is about to enter the clogging state.

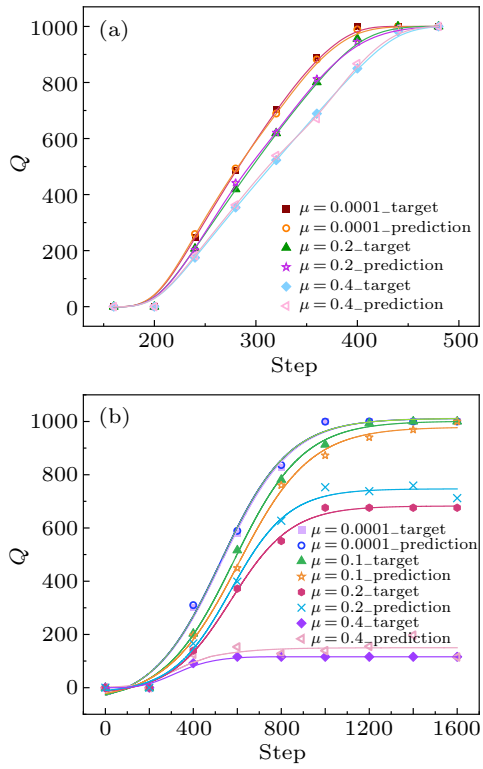


Fig. 5. Predicted results of the GDAnet model for granular flow simulation data for different friction scenarios. Panel (a) shows the case without clogging for a funnel caliber of 2.0 and panel (b) shows the case with clogging present for a funnel caliber of 0.8.

This ability to detect the abnormal state (blockage) is difficult to realize with traditional single-point prediction and has an important early warning value. In the case of blockage, the prediction error stems primarily from the model's attempt to assign a finite time value to a process that is essentially stagnant (of infinite duration). The fact that the model predictions are significantly higher than the normal range in the absence of blockage is in itself a strong indication that blockage is occurring. Its 'reasonable margin of error' is reflected in the model's ability to reliably distinguish between the distribution of predicted values in the blocked and non-blocked states. According to the comparison of the fitted curves of the prediction results under different friction conditions as shown in Fig. 5, although the clogging problem leads to the error between the prediction results and the real value, on the whole, the fitted curves of the prediction effect of the GDAnet model can still clearly reflect the clogging tendency of the system under the corresponding conditions and have a reasonable range of error interpretability.

4. Conclusion

This paper develops a GDAnet deep learning model trained on LAMMPS simulation data to enable cross-scale prediction of granular flow, encompassing both static snapshots and dynamic processes. The model predicts instantaneous outflow times with a high coefficient of determination (R^2 = 0.992) and accurately identifies dynamic flow patterns, achieving overall prediction accuracies exceeding 90%. Furthermore, a distinct clogging state was identified during the dynamic recognition process. The model effectively predicts both clogging and circulation states under varying friction conditions, thereby accurately reflecting clogging tendencies with a justifiable margin of error. Prediction errors partly arise from the inherent complexity of the physical processes, including phase transition ambiguities and the stochastic nature of blockages, as well as data limitations. These challenges highlight the need for integrating more refined physical models or uncertainty quantification methods in future work.

Methodologically, GDAnet independently extracts and refines spatial and temporal features through a spatiotemporal feature decoupling architecture, effectively addressing the challenges of cross-scale modeling and improving the ability to capture key physical characteristics. The model integrates data-driven learning with prior physical knowledge, enabling application to domain-specific scenarios such as funnel flow while maintaining strong generalization performance. This research establishes a novel computational paradigm for analyzing granular matter dynamics and advances the application of deep learning in modeling complex physical systems.

Despite the promising performance of GDAnet, the current study is limited to 2D images and spherical particles, which may not fully capture the complexities of real-world granular flows involving non-spherical particles and three-dimensional dynamics. To extend the method to more realis-

tic scenarios, future work could incorporate 3D imaging techniques and employ 3D convolutional neural networks (3D-CNNs) or voxel-based representations to capture spatial features in three dimensions. Additionally, particle shape descriptors or graph neural networks could be integrated to model non-spherical granular interactions. Such extensions would enhance the model's applicability in industrial settings where particle morphology and 3D flow behavior are critical.

Acknowledgements

Project supported by the National Natural Science Foundation of China (Grant No. 11702289), the One Hundred Talent Project of the Chinese Academy of Sciences (Grant No. Y5ZKRCGZ01), and the Science and Technology Commission of Shanghai under the Second Batch of the 2024 Annual Science and Technology Innovation Action Plan in the Field of Aerospace and Marine Science and Technology (Grant No. 24DZ3101402).

References

[1] Pezo M, Pezo L, Lončar B, Kojić P, Ilić M and Jovanović A 2025 2025 *Powder Technology* **459** 121040
[2] Adamczyk W, Widuch A, Morkisz P, Zhou M, Myöhänen K, Klimanek A and Pawlak S 2024 *Powder Technology* **444** 120006
[3] Debnath B, Kumaran V and Rao K K 2024 *Powder Technology* **431** 119036
[4] Drake T G 1991 *Journal of Fluid Mechanics* **225** 121
[5] Hawkins G 1983 Simulation of granular flow *Studies in Applied Mechanics*, Vol. 7 (Elsevier) pp. 305–312
[6] Shan T R, Thompson A P and Plimpton S J 2013 *Large-scale molecular dynamics simulations with lammps. Tech. Rep.* Sandia National Lab. (SNL-NM), Albuquerque, NM (USA)
[7] Thompson A P, Aktulga H M, Berger R, Bolintineanu D S, Brown W M, Crozier P S, In't Veld P J, Kohlmeyer A, Moore S G, Nguyen T D, *et al.* 2022 *Comput. Phys. Commun.* **271** 108171
[8] Filipe H A and Loura L M 2022 *Molecules* **27** 2105
[9] Campbell C S and Brennen C E 1985 *Journal of Fluid Mechanics* **151** 167
[10] Hollingsworth S A and Dror R O 2018 *Neuron* **99** 1129
[11] Mujumdar A, Robi P, Malik M and Horio M 2007 *International Journal for Computational Methods in Engineering Science and Mechanics* **8** 149
[12] Cui Y, Fang J, Li Y and Liu H 2022 *Engineering Geology* **306** 106742
[13] Zhang Y, Wang X, Wang Y and Zheng W 2024 *Chin. Phys. B* **33** 070702
[14] Liu Y, Wang R, Zhao C and Zheng W 2022 *Chin. Phys. B* **31** 116401
[15] Zhao H, Wang R, Zhao C and Zheng W 2023 *Chin. Phys. B* **32** 056402
[16] Bourilkov D 2019 *Int. J. Mod. Phys. A* **34** 1930019
[17] Wang R, Kashinath K, Mustafa M, Albert A and Yu R 2020 *Proceedings of the* 26*th ACM SIGKDD international conference on knowledge discovery & data mining* pp. 1457–1466
[18] Lu L, Gao X, Dietiker J F, Shahnam M and Rogers W A 2021 *Chemical Engineering Science* **245** 116832
[19] Qu T, Di S, Feng Y, Wang M and Zhao T 2021 *International Journal of Plasticity* **144** 103046
[20] Cui J, Li Y, Zhao C and Zheng W 2023 *Chin. Phys. B* **32** 096101
[21] Zhang P and Yin Z Y 2021 *Computer Methods in Applied Mechanics and Engineering* **382** 113858
[22] Wang R, Fang F, Cui J and Zheng W 2022 *Sci. Rep.* **12** 500
[23] Xu D and Shen Y 2022 *Chemical Engineering Journal* **450** 138036
[24] Krizhevsky A, Sutskever I and Hinton G E 2017 *Communications of the ACM* **60** 84
[25] Alzubaidi L, Zhang J, Humaidi A J, Al-Dujaili A, Duan Y, Al-Shamma O, Santamaría J, Fadhel M A, Al-Amidie M and Farhan L 2021 *Journal of Big Data* **8** 1
[26] Kattenborn T, Leitloff J, Schiefer F and Hinz S 2021 *ISPRS Journal of Photogrammetry and Remote Sensing* **173** 24
[27] Wu Z and He S 2021 *Iranian Journal of Science and Technology, Transactions of Electrical Engineering* **45** 493
[28] Ismail Fawaz H, Lucas B, Forestier G, Pelletier C, Schmidt D F, Weber J, Webb G I, Idoumghar L, Muller P A and Petitjean F 2020 *Data Mining and Knowledge Discovery* **34** 1936
[29] Rothe R, Timofte R and Van Gool L 2015 *Proceedings of the IEEE international conference on computer vision workshops* pp. 10–15
[30] Rothe R, Timofte R and Van Gool L 2018 *International Journal of Computer Vision* **126** 144